SPS2022
A.H.C. Ng et al. (Eds.)

doi:10.3233/ATDE220175

Microstructural and Mechanical Properties of Polylactic Acid /Tin Bronze Tensile Strength Bars Additive Manufactured by Fused Deposition Modelling

Senad Dizdar[1] and Amogh Vedantha Krishna
Halmstad University, Box 823, 301 18 Halmstad, Sweden

Abstract: Tensile stress bar samples have been additive manufactured by fused deposition modelling (FDM) route by using polylactic acid (PLA)/tin bronze filament, thermal de-binding and air sintering. The samples reach sintered density of 7.42 g/cm^3 or 85% of the relative density of the continuously casted CuSn10 reference. Tensile stress testing of the samples shows rather moderate mechanical properties, about half yield strength and one third maximal strength, elongation and hardness of the reference. Increase in the sample core density and elimination of large, agglomerated pores may result in largest improvement of the mechanical properties.

Keywords: Additive manufacturing (AM), fused deposition modelling (FDM), 3D-printing, polylactic acid (PLA), bronze, de-binding, sintering

1. Introduction

1.1. Tin Bronze and additive manufacturing

Tin bronze is one of the oldest metal alloys in use by humans, dated to about 3500 years BC. It is an important development step in early manufacturing technology since the tin bronze's moderately high melting point and high mechanical strength allows manufacture of tools, weapons, jewelry, art pieces, dishes etc. [1]. In 17th century, the industrial revolution takes place and tin bronze plays an important role as a material for industrial applications such as bearings and gears where the tin bronze parts gain low friction and wear in contact with steel counter parts. Nowadays, tin bronze might be unfairly considered as a mature and redundant metal alloy, but its performances are not yet matched for many industrial applications. Considering manufacture of tin bronze components, a common manufacturing route consists of component/continuous casting and various chip machining operations. Material utilization due to the chip machining can be rather low resulting in high cost of discarded material. Its recycling – remelting requests additional energy, pollutes the environment and increases CO_2-trace. Recent efforts of our global society on reducing global warming up of the Earth, demand the high material utilization and highly effective recycling. Introduction of additive manufacturing (AM) in late 20th century offers a way to increase the material utilization. That is because the chip

[1] Corresponding Author: senad.dizdar@hh.se

machining is no longer aimed for removal of relatively large amounts of the bulk material but for removal of the rather small amounts to achieve dimension and form tolerances of the components. In other words, sustainability of the tin bronze components increases.

AM (Gibson et al. [2]) offer a few technologies for manufacture of tin bronze parts. Powder bed fusion (PBF) (Gibson et al.[2]) such as selective laser sintering (SLS) and selective laser melting (SLM) use tin bronze powder while material extrusion such as fused deposition modelling (FDM) called also fused filament fabrication (FFF), uses filament or pellets made of tin bronze (Gibson et al.[2], Steuben et al.[3]). SLS and SLM technologies are one-step processes (excluding finishing) and achieve high respective full density tin bronze parts with a high cost/performance ratio. However, some limitations come with the parts' small to moderate size due to the powder bed principle and rather high reflectivity of the laser light comparing to stainless steels for example (Gibson et al. [2]). On other side, metal-FDM includes three steps, 3D-printing, de-binding and sintering similar to metal injection molding technology (MIM) in powder metallurgy (PM). However, FDM can manufacture parts with high density and a quite high cost/performance ratio for lower process cost and much lower capital investment in equipment in comparison to both SLS/SLM and MIM technologies at least for small and moderate product series. Tin bronze CuSn10 is quite often used for both SLM and FDM technologies due to reasons such as powder/filament availability on the world market.

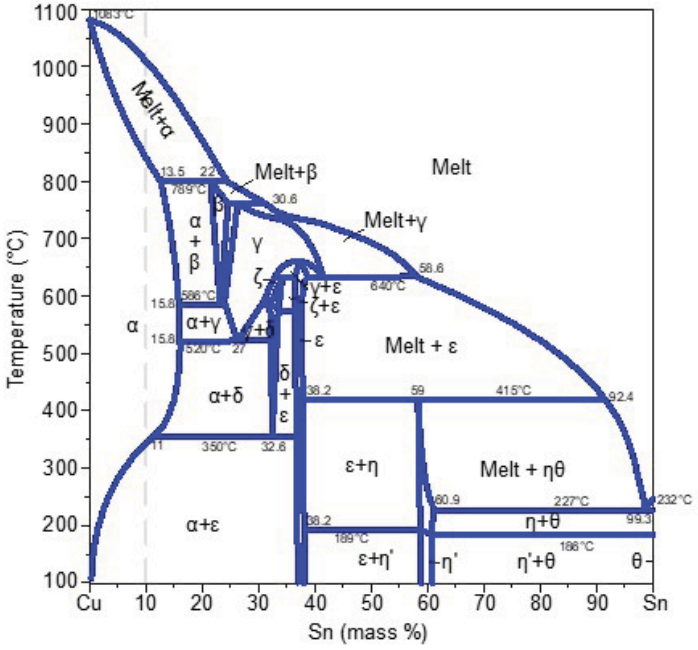

Figure 1. Phase diagram copper- zinc (Cu-Sn), redrawn based on e.g. [4], [9].

DIN EN CuSn10 bronze (also designated as 90/10 bronze, UNS C90700, SAE 65) is a common bronze alloy with nominally 90 % copper and 10 % tin. It is used for manufacture of components such as gears for high sliding velocities, bearings for relatively high loads and low sliding speeds, then bushings, piston rings, fittings, industrial valves' housings etc. [4]. For the most, two specifications of elemental composition are in use, one according to DIN EN 1982 [5] and another according to UNS C90700/SAE 65 [4], see Table 1. Small addition of phosphorus as a deoxidant in the melting process improves

wear resistance and stiffness (Gleaser [6]). Small additions of lead increase machinability and self-lubricating properties of the tin bronze but the well-known toxicity of the lead (e.g. EU Reach regulation [7]) needs to be taken into account. The nominal melting temperatures of the CuSn10 are approximately 830°C (solidus) and 1000°C (liquidus), see copper-tin phase diagram in Figure 1 (e.g. [4], Saunders et al. [9]).

Table 1. Elemental composition of CuSn10 bronze.

	Elemental composition (mass %)											
	Cu	**Ni**	**P**	**Pb**	**Sn**	**Al**	**Fe**	**Mn**	**S**	**Sb**	**Si**	**Zn**
DIN EN 1982 [4]	88-90	<2	<0.2	<0.1	9-11	<0.01	<0.2	<0.10	<0.05	<0.2	<0.02	< 0.05
UNS C90700, [2]	88-90	<0.5	<0.3 *	<0.5	10-12	< 0.005	<0.15	-	<0.05	<0.2	< 0.005	< 0.50

* P< 1.5% for continuous casting.

Table 2. Mechanical properties of CuSn10 bronze.

Description	**Yield strength**	**Max. strength**	**Strain at max. str.**	**Elast. module**	**Hardness**	**Spec. dens.**	**Ref.**
	$R_{p0.2}$ (MPa)	R_m (MPa)	ε_m (%)	E (GPa)		(g/cm^3)	
CuSn10-GC	>170	>280	>10	90-110	>80 HBW	8.7	DIN EN 1982 [5]
C90700 (cont. cast)	>172	>276	>10	103	-	(8.77)	Deng [11]
CuSn10-GC [1]	170	360	6	-	55 HRB	8.6	Deng [11]
CuSn10 (SLM [2])	369	433	14	-	76 HRB	8.8	Deng [11]
CuSn10 (SLM [3])	399	490	19	-	77 HRB	8.9	Deng [11]
CuSn10 (SLM [4])	390	486	15	-	75 HRB	8.7	Deng [11]
CuSn10 (SLM)	-	528	13	-	155 HV	-	Ruinan [10]
CuSn10 (SLM[4])	220	420	17		-		Scudino [12]

[1] Chinese ind. standard YS/T 545-2006, [2] 210 J/mm^2, [3] 220 J/mm^2, [4] 230 J/mm^2, [5] 217 W

Mechanical components made of tin bronze achieve high mechanical strength, low friction coefficient and high wear resistance in sliding against steel, high electrical and thermal conductivity as well as high resistance to sea water, acidic and other corrosive environments (Ashby [1], Glaeser [6]). Table 2 lists mechanical properties of CuSn10 as continuous cast, the most often occurring form at the market [5]. Ruinan et al. [10] and Deng et al. [11] investigate feasibility of SLM for component manufacture. They print TS-bars and perform tensile testing on them. Their results show in comparison to continuously casted CuSn10, about 50-90% higher max. strength R_m, about 15-35% higher yield strength $R_{p0.2}$, and about 30-90% higher elongation. Hardness cannot be compared because of different hardness methods and absence of relevant conversion tables. That difference in mechanical properties could be explained by the two ten powers difference in cooling rate, about 10^4 °C/s for SLM compared to 10^2 °C/s for continuous casting (Deng et al. [11]). Lu [12] reports FDM feasibility studies where they 3D-print TS-bars

from a polylactic acid (PLA)/copper filament by TVF and some other metal filaments, perform air de-binding and air-sintering but do not perform the tensile testing. Ayeni [14] reports a FDM feasibility study of a PLA/ CuSn10 bronze filament by TVF and use tensile and bending bars as test samples. The sintering performs at 832°C, a former recommendation from TVF, and results sintered bronze samples but quite brittle ones with elasticity module from bending testing of only 107 MPa.

1.2. FDM technology

The first step in metal-FDM technology, 3D-printing, needs to provide printed parts of a high quality to de-binding and sintering steps. Basic demands on the printed parts are high printed (green) density, small and evenly distributed pores over the cross section, and absence of large, agglomerated pores. If these demands are fulfilled, the parts may achieve a high mechanical strength. In addition, having the parts' surface layer with full or high density will improve resistance to surface related phenomena, such as wear and corrosion. To fulfill all these demands, numerous parameters need to be fine-tuned. Figure 2 (Steuben et al. [4]) shows a principal sketch of FDM 3D-printing. Filament feedstock comes from a spool into an extruder body. An extruder drive gear feeds the filament into a heater to get it heated up, then squeeze it through a nozzle and finally deposit it in form of a string onto a build plate with or without previously deposited strings. The deposition proceeds from the part bottom layer(s) layer-wise in vertical direction, with perimeter strings for outer surface of the part in two horizontal directions, infill strings for cross section filling, and the part top layer(s). The bottom, top and perimeter layers are normally solid while the infill layers are sparse with rectilinear, grid, honeycomb or other patterns. Of crucial importance is to select a proper extrusion string overlap between perimeter, infill and perimeter to infill strings (Figure 2).

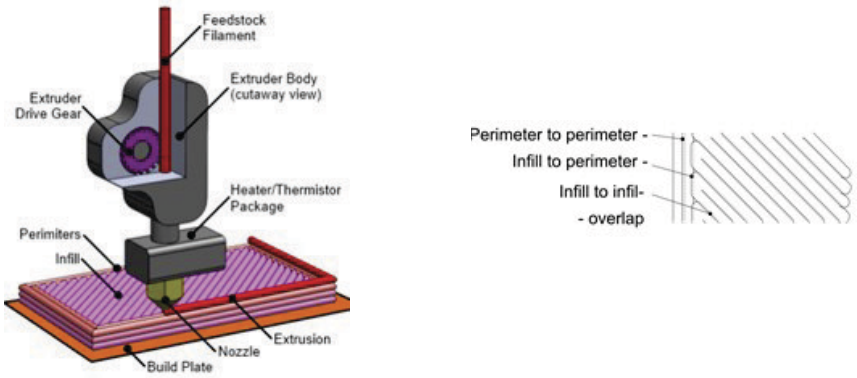

Figure 2. A principal sketch of FDM 3D-printing (left, Steuben et al. [3], used with permission of ASME) and top view of the contact between infill and perimeter extrusion strings (right).

Suteja et al. [17] review how various FDM 3D-printing parameters affect mechanical properties of the PLA 3D printed parts. Small layer thickness, dense infill density, high but not too high extrusion temperature and small cavities positively affect the mechanical properties. These parameters get a brief description here.

Layer thickness parameter, the height of each successive material layer deposited during the printing process, is likely the strongest factor affecting the surface quality and mechanical properties of the printed parts. As a rule of thumb, the larger the layer

thickness the larger gaps between the layers. This creates more pores between the layers and directly drops the density and tensile strength of the parts (e.g., Shubham et al. [18], Lu [12], Gante et al. [19]). A layer thickness of 0.1 mm provides a good quote between the mechanical properties and the printing time. PruseSlicer software [20] that prepares 3D-solid models for 3D-printing, associates 0.1 mm layer thickness as "fine quality".

Infill pattern parameters refers to the filling core structure of the part. The pattern infill density may vary between 40%-100% while the infill pattern form varies depending on the part's target strength to mass ratio. The raster angle, the angle between the travelling path direction of the print head and X-axis of the printing platform, can be adjusted to match specific loading directions. Ćwikła et al. [21] and Dudescu et al. [22] illustrate how infill pattern and infill raster angle of ABS plastic FDM parts affect the mechanical properties. Damon et al. [21] showed the effect of infill pattern and raster angle for sintered FDM TS-bar samples of a POM/316L filament.

Ironing parameters describe how the nozzle travels repeatedly over the top surface of the printed part with reduced material flow such as 30%. It smoothens and selectively densify the part top surface to its virtually full density. It also reduces the surface roughness and the raster lines visible during the printing process. Accordingly, the ironing is an important feature for surface related properties, such as tribological, corrosional and aesthetic ones. PrusaSlicer [20] allows this operation so far only on the top flat surface.

Perimeter parameter denotes number of outer contour-shell extension strings of the printed parts. It contributes to a denser part surface and affects the surface related properties in similar way as the ironing. Sukindar et al. [24] show that a high number of perimeters increases the tensile strength of the printed parts with lower infill percentages.

The print speed in this study is lower than the recommended, mainly to ensure a good dimensional and surface quality. The print temperature is slightly higher than the recommended one for PLA-metal filaments because as the hardened steel nozzle has slightly lower thermal conductivity than the typical brass nozzles. Hardened steel nozzles offer high wear resistance with benefits for extrusion of PLA/bronze filaments.

The extrusion multiplier parameter refers to the material flow rate during the printing process. Filaments with a higher abrasivity, such as PLA/bronze-ones, can cause severe wear of the Teflon tube situated inside the print head and uneven material flow. To avoid it, the material flow rate was set to 30% more than the regular value.

Typically, the metal powder size distribution in metal-infused PLA filaments ranges from 50 to 150 μm but sometimes up to 400 μm. To avoid the nozzle clogging during the printing process, the nozzle diameter is kept at 0.6 mm.

In a quite strong analogy with the parts manufactured PM and MIM, FDM parts needs to be first de-bound and then sintered. Burkhardt et al. [25] illustrate the MIM-FDM analogy on plate samples made of 316L filament respectively pellets with undisclosed binder. The samples are de-bound by using solvent de-binding and thermal de-binding integrated with (undisclosed) sintering. Contreras et al. [26] report a MIM study on 90/10 bronze part with different powder characteristic. The extruded, green 90/10 bronze parts are firstly solvent de-bound in hexane and then thermally de-bound and sintered in hydrogen atmosphere at 870°C. They point out importance of solvent de-binding to remove the surface binder and open exhaust channels for later thermal de-binding of the binder in the part core structure. TVF recommends thermal de-binding of parts submerged in tabular alumina at 482°C for three hours for their PLA-based binder in their bronze-filament [16].

Sintering of FDM CuSn10 parts can follow praxis in PM and MIM. CuSn10 sintering performs in common as super solidus liquid phase (SSLP) sintering (German [27]).

The SSLP sintering goes on a temperature between the solidus and liquidus temperatures for an alloy. For CuSn10, the solidus temperature is 830°C and the liquidus one is 1050°C, see the Cu-Sn phase diagram in Figure 1, and a SSLP sintering temperature of 870°C is reported (Contreras et al. [26], German [27]). Sintering heating rate is in common 5°C/s and sintering time depends on the sintering atmosphere. For air sintering TVF recommends the sintering time of three hours. To protect the hot CuSn10 parts from oxidation and to speed up the deoxidation process, the thermal de-bound parts submerged into tabular alumina are covered with 25 mm layer of sintering carbon such as activated coal powder. The coal powder undergoes an incomplete combustion in the closed furnace chamber resulting in generation of CO gas that deoxidizes the Cu and Sn oxides present in the CuSn10 powder (German [27], Goldstein [28]).

FDM with CuSn10 material - commercial filament is present on the world market likewise 3D printing, de-binding and sintering equipment while literature as cited above describes details of the manufacturing steps. However, feasibility studies illustrating the CuSn10 FDM process and the achieved mechanical properties are few. A reported FDM feasibility study by using a PLA/CuSn10 filament proves achievement of sintered bronze, but the very low mechanical properties suggest a rather moderate outcome (Ayeni [14]).

Investigation to be reported in this paper aims to perform a basic feasibility study of FDM manufacturing by using a PLA/CuSn10 bronze filament. Based on the findings from the literature study as above, standard TS-bar samples are made by 3D-printing, thermal de-binding, and air-sintering. All the steps are to be documented, analyzed, and compared to references. Standard tensile and hardness testing are performed to illustrate basic mechanical properties. The achieved mechanical properties are to be compared with reference cast CuSn10 and results of SLM investigations of CuSn10 (Table 2).

2. Material and experiment

TS-bars selected for this investigation are of 1BA type from ISO 527-2 [2]. This type is one of few recommended for extruded thermoplastic materials including filled and reinforced compounds. FDM is otherwise classified as a material extrusion 3D-printing technology. FDM manufacturing route of TS-bar samples consists of 3D-printing with PLA/bronze filament, thermal de-binding, air sintering and gentle glass ball blasting. Table 4 lists more details on consumables and equipment used in the manufacturing route.

3-D printing follows and takes into account recommendation by the 3D-printers producer (PrusaSlicer [20]), the filament producer TVF (MSDS [15]), TDS [16]) and findings from reports [17]-[23]. The intention is to achieve as printed – green TS-samples with a high density i.e., a low porosity that ensures safely handling with the green samples and that is a prerequisite for a good sintering.

Table 5 lists settings of the printer (Prusa MK3S) equipped with a ø0.6 mm hardened steel nozzle to improve printability and reduce nozzle wear. The layer height is 0.1 mm for fine quality prints (PrusaSlicer [20]). The infill density is 100%, towards full part core density, with 45° raster angle rectilinear pattern, 12.5% infill overlap and 0.675 mm extrusion width (equal to 1.125 times of the nozzle size). The PrusaSlicer allows so far only the rectilinear pattern for 100% infill. The perimeter strings are 4, the infill to perimeter overlap is 25%. The ironing is enabled with 30% flow rate. The print-, the travel- and the ironing speeds are 20, 80 and respectively 15 mm/min. The print and the bed temperatures are 220 respective 60°C. To compensate for the shrinkage, the printed bar width is set to 130%, the length and the height to 110% of the nominal size. The printed

samples are oriented along x-axis. In total, 10 samples are printed with 49 minutes print time per piece. A graphic tape (Conform 4075RLA) covers the printer's build platform plate to prevent its damages and to improve adhesion to the printed part.

Temperature vs. time of de-binding and sintering cycles is illustrated in Figure 4. The TS-bar samples are placed in a crucible tray, in-bedded and covered with the tabular alumina sand. The tray is placed in the middle of the furnace chamber. With heating rate of 5°C, the furnace goes up from the room temperature to thermal de-binding temperature of 482°C and keeps this temperature for 240 minutes. The tray gets shortly out of the furnace for covering with 25 mm activated coal powder and get back into the furnace. After that, using the same heating rate, the furnace goes up to sintering temperature of 870°C and keeps this temperature for 180 minutes. To mention again, this sintering is a super-solidus liquid phase sintering (German [27]). The tray with the TS-bar samples is left to cool down together with the furnace for about 22 hours. The cooling rate is about 3°C/min in the beginning and about 0.1 C/min in the end of the cooling

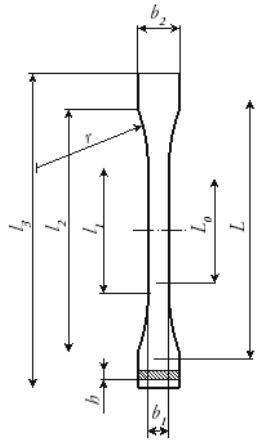

Figure 3 Drawing of tensile stress test bar according to ISO 527-2 type 1BA.

Table 3. Tensile stress test bars ISO 527-2 type 1BA

Dimension	**Value**
Overall length l_3 (mm)	≥75
Length of narrow parallel-sided portions l_1 (mm)	≥30
Radius r (mm)	≥30
Distance between broad parallel-sided portions l_2 (mm)	58±2
Width at the ends b_2 (mm)	10.0±0.5
Width at narrow portion b_1 (mm)	5.0±0.5
Thickness h (mm)	≥2
Gauge length L_0 (mm)	25.0±0.5
Initial distance between gaps L (mm)	$l_{2\,+0}{}^{+2}$

Table 4. Printer, filament, sintering consumables, and sintering furnace at FABLab of Halmstad Univ.

	Description	**Specific properties, as disclosed**
3D-printer	Original Prusa I3 MK3S+	
Filament	Bronze Filament™, (The Virtual Foundry)	ø1.75 mm; PLA base / metal 87.40% (mass); metal 90% Cu, 10% Sn; specific density 4.29 g/cm^3
Painter tape	(Conform 4075RLA)	Graphic tape with a high tack level
Activated charcoal	Coobra Kol (Vendor)	Particle size: 0.43–1.7 mm; spec. density≈ 0.47 g/cm^3, spec. surface area: 1050 m^2/g.
Alumina sand	Tabular alumina T-60 (Almantis)	0.5 – 1 mm (14 – 28 mesh)
Sintering furnace	Muffle furnace (Nabertherm L9/11/B170)	Air furnace, 9 l chamber capacity, max. temperature 1100°C.
Blasting unit	(No name)	Air pressure 6 bar, glass balls ø0.25-ø0.42 mm

Table 5. Printer settings – (Prusa MK3S)

Print setting	**Value**
Nozzle diameter | nozzle material	Ø 0.6 mm | hardened steel
Layer height | first layer height	0.1 mm | 0.1 mm
Infill density | pattern | angle	100 % | rectilinear | 45°
Infill overlap | extrusion width	12.5 % | 0.675 mm
Perimeter strings | Infill to perimeter overlap	4 | 25%
Ironing | ironing flow rate	Enabled | 30 %
Print speed | travel speed | ironing speed	20 mm/s | 80 mm/s | 15 mm/s
Extrusion multiplier	130%
Print temperature / bed temperature	220°C/ 60°C
TS-bars - scale factors Length 75 mm, X Width 5.5 mm, Y Height 2 mm, Z	Scaled 82.5 mm (110 %) 7.15 mm (130 %) 2.6 mm (130 %)
Orientation of the TS bars on the build platform	Along x-axis
Total printed TS bars | Print time/pc of TS bars	10 pcs | 49 min

The final manufacturing route step is blasting with glass balls. The blasting removes soot and in-soot-in-bedded alumina particles from the TS-bar samples. The blasting is gentle, to clean the sintered TS-bar samples and not to densify their surface.

Table 6 lists analysis and testing methods with corresponding equipment used in the investigation. These five analyses- and testing methods should provide a picture over all important aspects of the of test samples – density, porosity, sintering quality and basic mechanical properties.

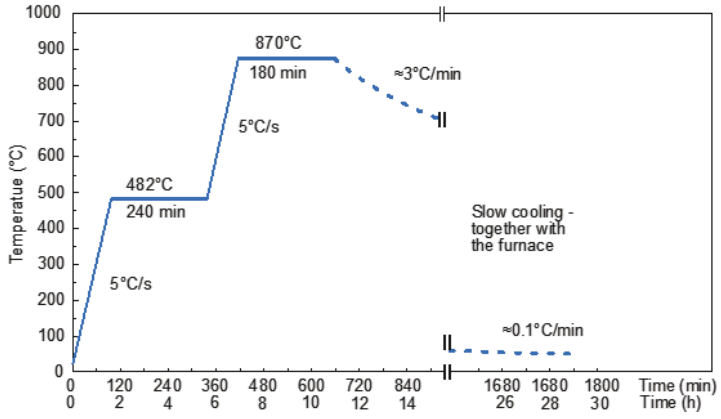

Figure 4. De-binding and sintering cycle for the TS-bars.

Table 6. Analysis and testing equipment used in the investigation

Analysis/testing	Description
Density evaluation	Archimedes method ASTM B962 [31], an analyt. balance (Radwag 750 g/1 mg)
Tensile testing	ISO 527 [30], a common tensile tester (MTS Exceede 100 kN, 10 kN load cell)
Hardness testing	Rockwell ISO 6508 [33], Brinell ISO 6506 [34], a hardness tester (Mitutoyo HR-530)
Metallography	SEM (Jeol JSM 6480LV / Ametek EDAX sensor, Genesys software)
Surface topography	ISO 25178 [32], a white light interferometer (WLI) (Zygo NewView 9000)

3. Results

A first step in assessment of the sintering outcome is to look at the TS-bar sample density and dimension (Table 7, Figure 5), overall appearance (Figure 7) and detailed appearance surface topography (Figure 8). As shown in Table 7, as printed TS-bar samples achieve 4.7 g/cm^3 in specific density what is slightly higher than the filament density 4.29 - 4.5 g/cm^3 [16]. A reason for it can be minor variations in porosity and metal powder content. The sintered TS-bar samples achieve 7.4 g/cm^3 in specific density or approximately 85% of CuSn10 full density. This is a moderate density, a relative density level of at least 90% would be targeting for structural components other than porous bearings or similar. To compare width, Damon et al. [23] achieved 316L-FDM TS-bars with relative density of higher than 98% but with catalytic de-binding and reactive gas atmosphere sintering. Dimensions of the TS-bar samples are scaled for 110%, 130% and 130% for respectively their length, neck width and thickness in comparison to the nominal 1BA ISO 527-2 TS-bar samples. The printed TS-bars achieve swelling/shrinkage after being taken out of the printer board and cooled to the room temperature and achieve 110%, 136% respectively 125% of the nominal samples. Finally, the sintered TS-bars achieve 108%, 107% respectively 105% of the nominal sample dimensions.

Evaluation of the sintered density suggests one important point. The TS-bar samples do not take in water. This can be hardly possible when the relative density is at the level of 85% unless the surface is sealed in some way. Figure 5 shows SEM view of two SEM cross sections of a TS-bar sample. As seen, the surface of all four outer sides of the TS-bar is not having surface pores interconnected with the core material due to the ironing and 4 perimeter strings. The core material volume includes large, aggregated pores but these pores do not reach the surface.

Table 7. Density and dimensions of ISO 527-2 TS-bar samples, average values based on 10 replicas.

TS-bars	Nom. sample	Scaled	Printed	Sintered
Density (g/cm^3)		-	4.7	7.4 (85% full dens).
Length, X (mm)	75	82.5 (110%)	82.8 (110%)	80.8 (108%)
Neck width, Y (mm)	5.5	7.15 (130%)	7.5 (136%)	5.9 (107%)
Thickness, Z (mm)	2	2.6 (130%)	2.5 (125%)	2.1 (105%)

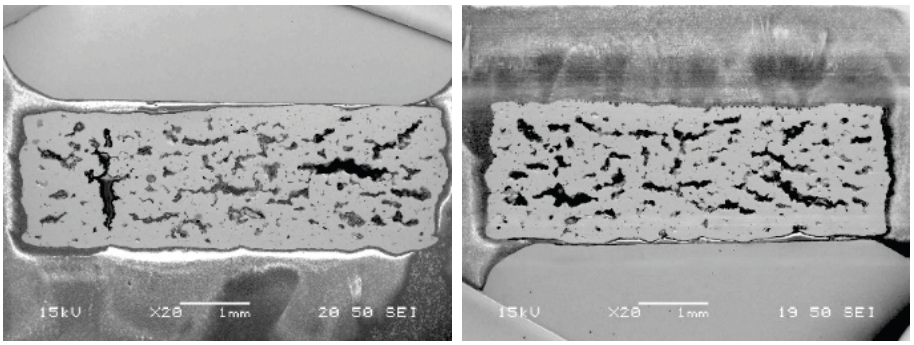

Porosity 13% Porosity 23%

Figure 5. SEM view of three cross sections of a FDM 3d printed and sintered bronze TS-bar.

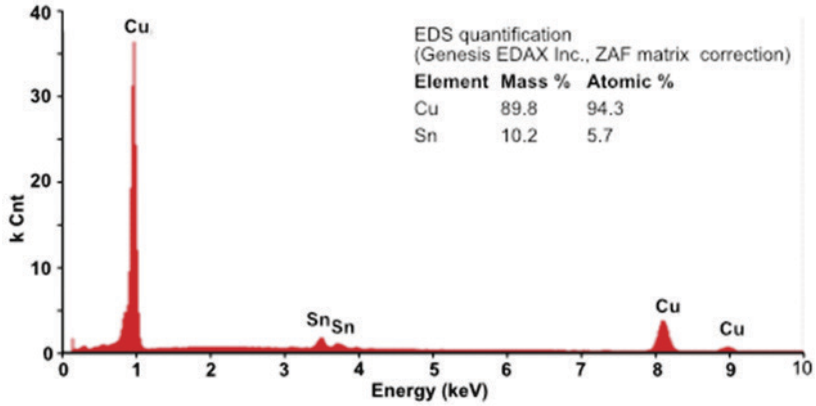

Figure 6. EDS elemental spectrum and quantification.

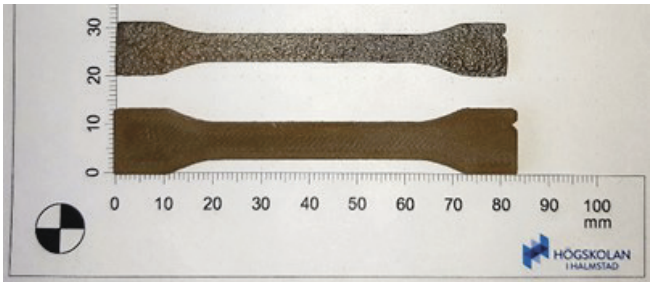

Figure 7. Appearance of TS-bar samples as de-bound (bottom) and as sintered (top).

Results of energy-dispersive X-ray spectroscopy (EDS) analysis of a TS-bar sample are shown in Figure 6. Cu and Sn peaks are very strong while peaks of other metal constituents cannot be distinguished from the background noise. Elemental quantification confirms that the sintered sample has composition equivalent to the filament nominal one, 89.8% Cu and 10.2% Sn i.e., CuSn10.

The sintered TS-bar samples (see Figure 7) show a metallic cast-sintered surface with a mixed bronzish - greyish appearance (greyish due to burning of the activated coal).

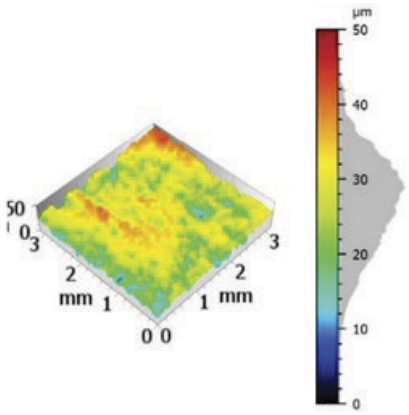

a) Printed, bottom, S_a=3.0, S_{10z}=28.9µm.

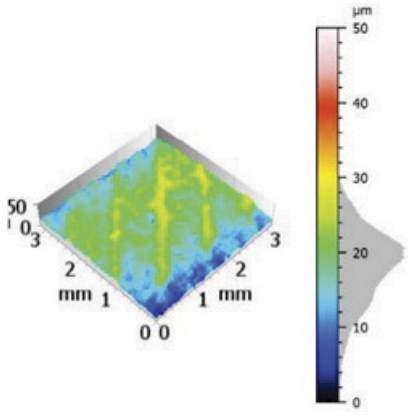

b) Printed, top, S_a=1.8 µm, S_{10z}=24.5 µm.

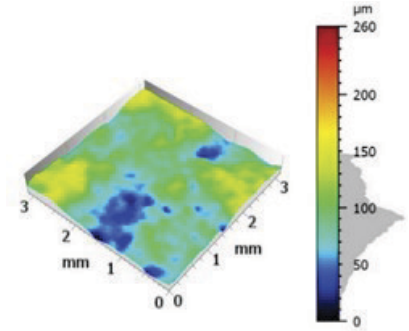

a) Sintered, bottom, S_a=6.8 µm, S_{10z}=75.6 µm.

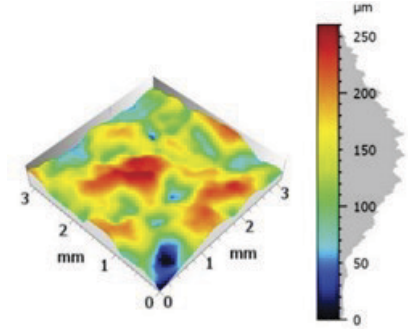

b) Sintered, top, S_a=13.0 µm, S_{10z}=122 µm.

Figure 8. Three-dimensional topography appearance of as FDM-3D printed and sintered TS-bars.

The de-bound TS-bar sample show as typical damped bronze appearance. Surface topography view of the TS-bar sample printed surfaces (see Figure 8) shows quite fine surfaces, average roughness S_a=3.0 µm, ten-point-height S_{10z}=28.9 µm for the bottom side and S_a=1.8 µm, S_{10z}=24.5 µm for the top side. To note that the bottom surface includes residuals of the painter tape from the printer print board (the residuals that cannot be removed by gentle scraping and ethanol rinsing). These residuals likely makes that the bottom surface seems slightly rougher than the top surface. The top side surface show infill 45° pattern also seen in Figure 7. The sintered TS-bar sample surface has a typical appearance of a sintered powder metallurgy metal surface with surface pores. The bottom side surface is almost twice finer, S_a=6.8 µm, S_{10z}=75.6 µm, compared to the top side surface, S_a=13.0 µm, S_{10z}=122 µm.

A next part in the evaluation of the sintered TS-bar samples is tensile testing, see Table 8. The yield - and the maximal strength are 82 respective 127 MPa and it is slightly less than 50% of these strengths for CuSn10 continuously casting reference. The strain at maximal strength and elasticity module, 3.63% respective 37.2 GPa, are slightly more than one third of the reference. Of course, to note that the sintered density is 7.4 g/cm^3 or 85% of the reference. The results are an indication since lognormal probability plot of the data shows quality of fit of 0.85 (at least 0.90 for a good fit). Figure 9 presents a SEM view over ductile fracture of a broken TS-bar sample and a close-up with typical dimples

and tearing features. It proves relevancy of the tensile testing. Presence of the large, aggregated pores across the TS-bar cross section, as already shown in Figure 5, is also seen here. The tensile test results here are as expected much lower in comparison with results for the SLM manufactured samples (Table 2), due to their virtually full relative density and fine-grain microstructure by a high cooling velocity.

Hardness of the sintered TS-bar samples is evaluated by using Rockwell [33] and Brinell [34] methods. To minimize measurement bias due to relatively high roughness, indentation proceeds on the finer, bottom side. Table 9 list the hardness results. For Rockwell hardness, a statistical check by lognormal probability plot returns a straight line with R^2-value of 0.96, mean hardness (P_{50}) of 49 HRLW with 10% (P_{10}) of the hardness data below 37 HRLW and 90% (P_{90}) below 65 HRLW. Corresponding indentation depth is 0.16 mm or about 8% of the sample thickness what comply with ASTM recommendation on of maximum 10% of the sample thickness. For Brinell hardness, the lognormal probability plot returns a straight line with R^2-value of 0.98, mean hardness of 30 HBW with 10% of the hardness data below 22 HBW and 90% below 42 HBW. The mean Brinell hardness here is about one third of the reference CuSn10 hardness (DIN EN 1982 [4]).

Table 8. Results of ISO 527 tensile stress testing on FDM 3D-printed, de-bound and sintered TS-bars ISO 527-2 made of Bronze filament™. (100 kN MTS Exceed® tensile tester, crosshead rate 15 mm/min, 5 replicas).

Yield strength	Max. strength	Strain at max. strength	Elasticity module	Spec. density
$\sigma_{y\,(0.2)}$ (MPa)	σ_m (MPa)	ε_m (%)	E (GPa)	(g/cm^3)
82.3±5.5	127.1±6.2	3.63±0.92	37.20±5.7	7.4 g/cm^3

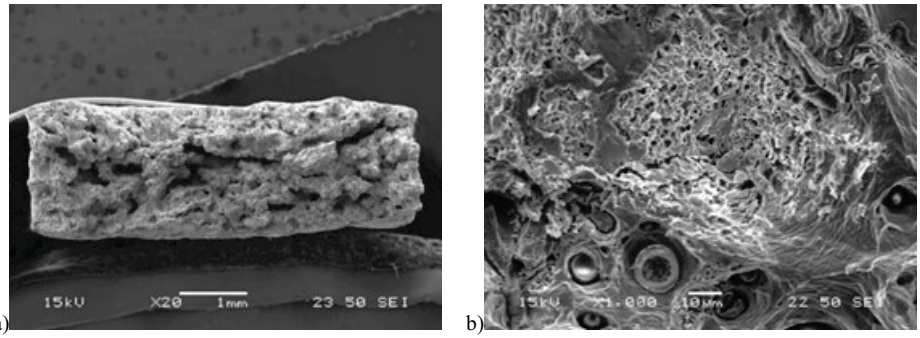

a) b)

Figure 9. SEM view over ductile fracture area of a broken TS-bar (a) and close-up of the fractured area with dimples and tearing features (b).

Table 9. Hardness of sintered Bronze FDM TS-bar samples, 6 replicas for HRLW and 14 replicas for HBW.

Method	Ball indenter (mm)	Loading	Hardness number
			P_{50}-mean | P_{10} | P_{90}
Rockwell HRLW	Ø6.35 mm (1/4“)	10/60 “kgf” ~ 98.1/588.6 N	49 | 37 | 65 HRLW
Brinell HBW	Ø10 mm	10/100 “kgf” ~ 98.1/981 N	30 | 22 | 42 HBW

4. Discussion

The moderate level of the mechanical properties of the FDM CuSn10 TS-bar samples, as de-bound and sintered, is of course unsatisfactory. Space for potential improvement is large. Largest improvement effects could come from increase in the core density by optimization of 3D-printing, binder alloying and de-binding/sintering. For 3D-printing is important to optimize wettability between the extrusion temperature, the extrusion strings, and their overlap. Here it may be an option to control occurrence of large, agglomerated pores. The de-binding and sintering can also be improved trough a better understanding of their mass and size effects.

The bronze-FDM manufacturing route with air sintering is an affordable and quite simple route that can find a wide use in micro-, small- and mid-sized enterprises. Also, the route meets the UN Sustainable Development Goals 8-12 (8-Decent work and economic growth, 9-Industri, innovation and infrastructure, 10-reduced inequalities, 11-sustainable cities and communities and 12-Responsible consumption and production).

5. Conclusions

Tensile strength (TS) bars have been FDM 3D printed from PLA / CuSn10 bronze filament, thermally de-bound at 482°C for 4 h, air sintered with activated charcoal cover layer at 870°C for 3 h and tensile tested. CuSn10 continuously casting is the reference technology. Following conclusion are met:

- TS-bar reach printed density of 4.7 g/cm^3 – over the nominal filament density of 4.29 - 4.5 g/cm^3.
- TS-bars reach sintered density of 7.42 g/cm^3 or 85% relative density. The core density includes large, agglomerated pores while the surface layer density is almost full due to the ironing in the 3D-printing and a proper number of the perimeter strings.
- Ironing and perimeter strings features of FDM-3D printing produce full dense surface layer beneficial for strength, tribology and corrosion performances.
- TS-bars achieve yield- and maximal strength of 82 respective 127 MPa are and it is about 50 % of the reference. The strain at maximal strength and elasticity module, 3.63 % respective 37.2 GPa, are about one third of the reference.
- TS-bars achieve mean hardness of 30 HBW or about one third of the reference.
- Surface roughness of the sintered TS-bar samples is S_a=6.8 µm/S_{10z}=75.6 µm for the printing bottom side and double, S_a=13.0 µm/ S_{10z}=122 µm for the printing top side.

Acknowledgements

The authors appreciate valuable discussion with prof. Bengt-Göran Rosén at Halmstad University, and all support by Tim Malmberg and Joakim Wahlberg at the FABLab.

References

[1] Ashby M.F., Materials selection in mechanical design: 4th ed., Butterworth-Heinemann, Amsterdam, 2011.

[2] Gibson I, Rosen D, Stucker BK, M. Additive Manufacturing Technologies: Springer International Publishing; 2021. XXIII, 675 p.
[3] Steuben J, Van Bossuyt DL, Turner C, Design for fused filament fabrication additive manufacturing. Inter. Design Eng. Tech. Conf. and Computers & Inf. Eng. Conf.; 2015; Boston, USA: ASME.
[4] C90700 SAE65 Gear Bronze / C907 High Tin bronze, National Bronze Manufacturing Co., nationalbronze.com as per August 2021.
[5] Kupfer-Zinn und Kupfer-Zinn-Zink-Gusslegierungen (Zinnbronze) - Informationsdruck i.25, Deutsches Kupferinstitut, Düsseldorf, 2004,
[6] Glaeser WA. Wear properties of heavy loaded copper-base bearing alloys. JOM-US. 1983;35(10):50-5.
[7] EU Reach regulation, echa.europa.eu/regulations/reach/understanding-reach.
[8] J.H. Shim, C.S. Oh, B.-J. Lee, D.N. Lee, Thermodynamic Assessment of the Cu-Sn System, Z. Metallkunde/Mater. Res. Adv. Tech., vol. 87, 1996, pp. 205-212.
[9] Saunders N, Miodownik AP. The Cu-Sn (Copper-Tin) system. Bulletin of Alloy Phase Diagrams. 1990;11(3):278-87.
[10] Ruinan Gu, Dawei Wang, Hui Wang, Ming Yan, Kam Sing Wong, Selective Laser Melting of Cu-10Sn-0.4P: Processing, Microstructure, Properties, and Brief Comparison with Additively Manufactured Cu-10Sn, Adv. Eng. Mater., 2021.
[11] Deng CY, Kang JW, Feng T, Feng YL, Wang X, Wu PY. Study on the Selective Laser Melting of CuSn10 Powder. Mater. 2018;11(4).
[12] Scudino S, Unterdörfer C, Prashanth KG, Attar H, Ellendt N, Uhlenwinkel V, et al. Additive manufacturing of Cu–10Sn bronze. Mater Lett. 2015;156:202-4.
[13] Lu H. Preliminary mechanical characterization of the low-cost metal 3D printing [Master Thesis]. Cookeville: Tennessee Technological University; 2020.
[14] Ayeni OI. Sintering and characterisation of 3D printed bronze metal filament [Master Thesis]. Indianapolis, Indiana: Purdue University; 2018.
[15] Bronze Filament™ - MSDS, The Virtual Foundry, Stoughton, 2020. www.thevirtualfoundry.com
[16] Bronze Filament™ - TDS, The Virtual Foundry, Stoughton, 2020., www.thevirtualfoundry.com.
[17] Suteja TJ, Soesanti A. Mechanical Properties of 3D Printed Polylactic Acid Product for Various Infill Design Parameters: A Review. J. Physics: Conf. Series. 2020;1569:042010.
[18] Shubham P, Sikidar A, Chand T., The influence of layer thickness on mechanical properties of the 3D printed ABS polymer by fused deposition modeling. Key Eng. Mater.; 2016: Trans Tech Publ.
[19] Gante LRK. Metal Filament 3D Printing of SS316L: Focusing on the printing process [Master Thesis]. Stockholm: KTH - Royal Institute of Technology; 2019.
[20] Prusa Slicer, www.prusa3d.com
[21] Ćwikła G, Grabowik C, Kalinowski K, Paprocka I, Ociepka P, The influence of printing parameters on selected mechanical properties of FDM/FFF 3D-printed parts. IOP Conf. Series: Mater. Sci. Eng.; 2017: IOP Publishing.
[22] Dudescu C, Racz L. Effects of raster orientation, infill rate and infill pattern on the mechanical properties of 3D printed materials. ACTA Universitatis Cibiniensis. 2017;69(1):23-30.
[23] Damon J, Dietrich S, Gorantla S, Popp U, Okolo B, Schulze V. Process porosity and mechanical performance of fused filament fabricated 316L stainless steel. Rapid Proto. J. 2019;25(7):1319-27.
[24] Sukindar NAB, Ariffin M, Baharudin B, Jaafar C, Ismail M. Analysis on the impact process parameters on tensile strength using 3d printer repetier-host software. ARPN J. Eng. Appl. Sci. 2017;12(10):3341-6.
[25] Burkhardt C, Freigassner P, Weber O, Imgrund P, Hampel S. Fused filament fabrication (FFF) of 316L Green Parts for the MIM process. World PM2016-AM-Deposition Techn. 2016.
[26] Contreras JM, Jiménez-Morales A, Torralba JM. Fabrication of bronze components by metal injection moulding using powders with different particle characteristics. J. Mater. Process. Techn. 2009;209(15):5618-25.
[27] German R. Sintering: From Empirical Observations to Scientific Principles: Elsevier Science; 2014.
[28] Peissker E. Sintered 90/10 bronze from powders with different tin contents. Met. Powder Report. 1983;38(5):259-62.
[29] Goldstein EA, Mitchell RE. Chemical kinetics of copper oxide reduction with carbon monoxide. P Combust Inst. 2011;33:2803-10.
[30] Plastics - Determination of tensile properties, ISO 527, 2019.
[31] Standard Test Methods for Density of Compacted or Sintered Powder Metallurgy (PM) Products Using Archimedes' Principle, ASTM B962, 2008.
[32] Geometrical product specifications (GPS) — Surface texture, ISO 25178, 2016
[33] Metallic materials — Rockwell hardness test, ISO 6508, 2017.
[34] Metallic materials — Brinell hardness test, ISO 6506, 2014.